Probing the acoustic phonon dispersion and sound velocity of graphene by Raman spectroscopy

Xin Cong [a, b], Qiao-Qiao Li [a], Xin Zhang [a], Miao-Ling Lin [a], Jiang-Bin Wu [a], Xue-Lu Liu [a, b], P. Venezuela [c], Ping-Heng Tan [a, b, *]

[a] *State Key Laboratory of Superlattices and Microstructures, Institute of Semiconductors, Chinese Academy of Sciences, Beijing 100083, China*
[b] *Center of Materials Science and Optoelectronics Engineering & CAS Center of Excellence in Topological Quantum Computation, University of Chinese Academy of Science, Beijing 100049, China*
[c] *Instituto de Física, Universidade Federal Fluminense, Niterói, Brazil*

ABSTRACT

The extraordinary thermal and elastic properties of graphene, mainly originating from its unique acoustic phonon branches near Γ point in Brillouin zone, have attracted great attention in its fundamental researches and practical applications. Here, we introduce an optical technique to accurately probe longitudinal acoustic (LA) and transverse acoustic (TA) phonon branches of graphene near Γ point by double resonant Raman scattering of the combination phonon modes in the range of $1650 - 2150\,cm^{-1}$ along with the overtone 2D' mode at $\sim 3200\,cm^{-1}$. The corresponding sound velocities ($v_{TA} = 12.9\,km/s, v_{LA} = 19.9\,km/s$) of graphene have been accessed, which are about 10% smaller than those of graphite. Based on v_{TA} and v_{LA}, the two-dimensional (2d) elastic stiffness (tension) coefficients c_{11} and c_{66}, Young's modulus Y_{2d} and Poisson's ratio σ_{2d} can be estimated. The results demonstrate again that double resonant Raman spectroscopy is a powerful tool to probe the fundamental properties of graphene.

© 2019 Elsevier Ltd. All rights reserved.

1. Introduction

The thermal and mechanical properties of graphene play a vital role in various graphene-based electronic, optoelectronic and nanoelectromechanical devices, such as field-effect transistors, flexible photodetectors, transparent strain sensor, ultrasensitive mass sensors and ultrahigh-frequency resonators [1]. In principle, thermal [2,3] and mechanical [4,5] properties of graphene have an inseparable relationship with acoustic phonons and their dispersion relations. The phonon dispersions of the longitudinal acoustic (LA) and transverse acoustic (TA) phonon branches of a material determine its longitudinal and transverse sound velocities (v_{LA} and v_{TA}), respectively, and further determine the Young's modulus. The acoustic phonon branches of some graphene-based materials, such as multilayer graphene flakes, carbon nanotubes and graphite have been investigated by Brillouin scattering (multilayer graphene) [6], inelastic X-ray scattering (graphite) [7], inelastic neutron scattering

(graphite) [8] and electron energy-loss spectroscopy (graphite) [9–11]. However, due to the limitations of measurement techniques, acoustic phonon branches of intrinsic graphene is difficult to be achieved by the above methods, and there are only a few theoretical reports on these properties of graphene [4,12,13]. Therefore, a convenient and direct technique to probe LA and TA phonon branches of graphene is necessary and pivotal for its both fundamental researches and practical applications.

Raman spectroscopy is a versatile tool for studying electronic, optical and phonon properties of graphene and graphene-based heterostructures and devices [14–16]. In general, due to the momentum conservation rule, the phonon at Γ ($q \sim 0$) point of Brillouin zone (BZ) can be probed by the first-order Raman scattering. The acoustic phonon is hard to be detected due to its ultralow energy at Γ. Fortunately, phonons with wavevector $q \neq 0$ in grahene-based materials can be activated by the double resonance (DR) or triple resonance (TR) Raman scattering [17,18]. For example, the frequency of the 2D mode, ω_{2D}, has been used to probe the transverse optical (TO) phonons near the K point of graphene-based materials via intervalley DR Raman scattering [14–18]. The DR Raman scattering related with acoustic phonons can provide a possible access to the LA and TA phonons in graphene-based

materials. Indeed, LA phonons of graphene near the K point have been probed via an intervalley DR Raman process of the D + D″ (∼ 2450 cm⁻¹) and 2D modes [19]. LA and TA phonons of graphite whisker [20], multiwalled carbon nanotubes [21], graphene [22] and bilayer graphene [23—26] near the Γ point have also been probed by DR Raman scattering and qualitatively agree with the corresponding theoretical calculation [18,27]. However, almost all the works can not provide the numerical values of the sound velocities of LA and TA phonons due to the limited experimental data points. In this case, it is difficult to compare the differences of acoustic phonon dispersions between graphene, graphite and other different graphene-based materials. Therefore, it is necessary to systematically probe the LA and TA phonons by DR Raman scattering technique with various excitation lasers as many as possible.

In this work, we investigated the two asymmetrical Raman peaks in the range from 1650 to 2150 cm⁻¹ with several excitation energies (E_i) from 1.59 eV to 2.81 eV. The two modes are assigned as the combination modes of the in-plane longitudinal optical (LO) phonons and LA (TA) phonons, whose frequencies are significantly dependent on E_i. The frequencies of LA ($\omega_{LA}(q)$) and TA ($\omega_{TA}(q)$) phonons as a function of wavevector (q) are probed via their intravalley DR Raman processes along with that of the 2D′ mode. The sound velocities and Young's modulus of graphene are deduced from the wavevector-dependent LA and TA phonon frequencies. This study has identified that the TA and LA sound velocities of graphene are about 10% smaller than those of graphite due to the presence of interlayer coupling in graphite.

2. Experiments and methods

The graphene sample was prepared by micromechanical cleavage of bulk graphite crystal and transferred to Si wafers with a 90 nm SiO₂ capping layer. The monolayer graphene flake is confirmed by its optical contrast and the lineshape of the 2D mode [28]. Raman measurements were performed at room temperature using a Jobin-Yvon HR800 system, equipped with several lasers and a liquid nitrogen-cooled charge-coupled detector (CCD). The Raman spectra are obtained by using a × 100 objective (numerical aperture of 0.90) and a 600 lines/mm grating under the backscattering configuration. The spectral resolution is 1.2 cm⁻¹ per CCD pixel at E_i = 1.96 eV. The excitation energies of the lasers are 1.59 eV from a Ti:Saphire laser, 1.96 eV from a He-Ne laser, 2.18, 2.52 and 2.67 eV from a Kr⁺ laser, 1.85 and 2.33 eV from a solid state laser, and 2.81 eV from a He-Cd laser.

Phonon frequencies have been calculated using ab-initio density functional theory (DFT) as implemented in the QUANTUM ESPRESSO code [29,30]. Single-particle wave-functions were expanded using an energy cutoff of 70 Ry and the Brillouin zone of graphene was sampled by 64 × 64 × 1 k-points in a Monkhorst-Pack grid. The ion-electrons interactions were described using the Projector Augmented-Wave method [31,32], local-density (LDA) and generalized-gradient (GGA) approximations. The small difference (a few meV) between phonon frequencies calculated using LDA and GGA are expected since LDA (GGA) overestimates (underestimates) binding energies.

3. Results and discussions

Fig. 1 depicts the Raman spectrum of graphene in the spectral region from 1450 to 3400 cm⁻¹ excited by E_i = 1.96 eV, including the G (∼ 1582 cm⁻¹), 2D (∼ 2630 cm⁻¹), D + D″ (∼ 2460 cm⁻¹) and 2D′ (∼ 3230 cm⁻¹) bands [14—16]. The G band corresponds to the doubly degenerate in-plane TO and LO phonons at Γ point of BZ. Both the 2D and 2D′ bands, corresponding to the overtones of the D and D′ bands, originate from the intervalley and intravalley TR
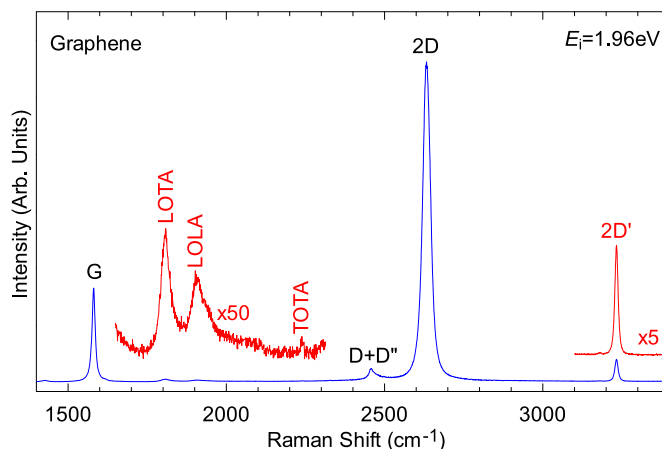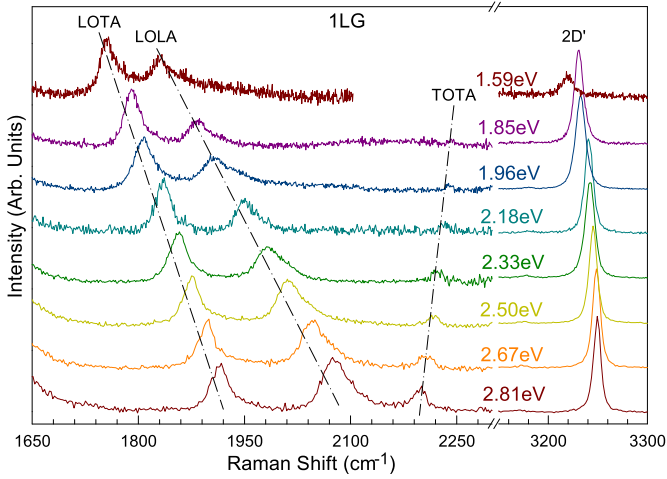

Fig. 1. Raman spectrum of graphene in the spectral range of 1450∼3400 cm⁻¹ excited by E_i = 1.96 eV. (A colour version of this figure can be viewed online.)

Raman processes, respectively. They show symmetric profile and can be fitted by a single Lorentzian peak. In contrast, the band at ∼ 2450 cm⁻¹, a combination mode of the D and D″ modes, exhibits asymmetric profile, which results from the intervalley DR Raman process [27]. Meanwhile, two weak peaks with asymmetric lineshapes are also observed in the spectral range from 1650 to 2150 cm⁻¹. Because their frequencies are larger than ω_G, the two peaks should be either overtones or combination modes of the LA, TA, LO and TO phonon branches near Γ or K points, which are activated in the Raman spectra by intravalley or intervalley DR Raman processes [16,27], respectively. Please note that, the TA branch [33] is also denoted as the shear horizontal (SH) branch [27], and the LO mode near Γ point and the TO mode near K point are denoted as the so-called D′ and D modes, respectively.

There are two possible resonance Raman processes for a combination mode, in which the two fundamental phonons are separately resonantly scattered [16]. To clearly distinguish the two components of the combination mode, in the denotation, the resonantly-scattered fundamental phonon is placed ahead, followed by the another fundamental phonon. For example, for the combination LO + LA mode, the wavevector of the fundamental LO and LA phonons is determined by the wavevector of the resonantly-scattered LO fundamental phonons, which is determined by the energy and momentum conservation rules in the Raman scattering process [16]. The two components of the combination mode can be generally denoted as the LOLA mode if it does not lead to misleading information. This denotation can be extended to other combination modes. According to the theoretical Raman spectra excited by the visible lasers [27], only the LOLA and LOTA modes locate in the spectral range of 1700 ∼ 2100 cm⁻¹. Therefore, the peaks at ∼ 1805 cm⁻¹ and ∼1905 cm⁻¹ can be assigned to the LOTA and LOLA modes, respectively. Indeed, similar LOLA and LOTA modes have been observed in graphite whiskers in this spectral range [20].

Fig. 2 shows Raman spectra of graphene excited by multiple lasers with E_i = 2.81, 2.67, 2.52, 2.33, 2.18, 1.96, 1.85 and 1.59 eV. It is noted that the abnormally low intensity of 2D′ peak with E_i = 1.59 eV results from the low quantum efficiency of CCD near corresponding detection wavelength. The intensity ratio of the LOTA and LOLA modes decreases with increasing E_i. The frequency difference between the two bands becomes smaller with decreasing E_i. Compared to the LOTA and LOLA modes, the 2D′ mode displays a smaller shift with decreasing E_i because it involves the LO phonon branch with more flat dispersion near Γ point [14,34]. An additional weak mode is also observed between ω_{LO+LA}
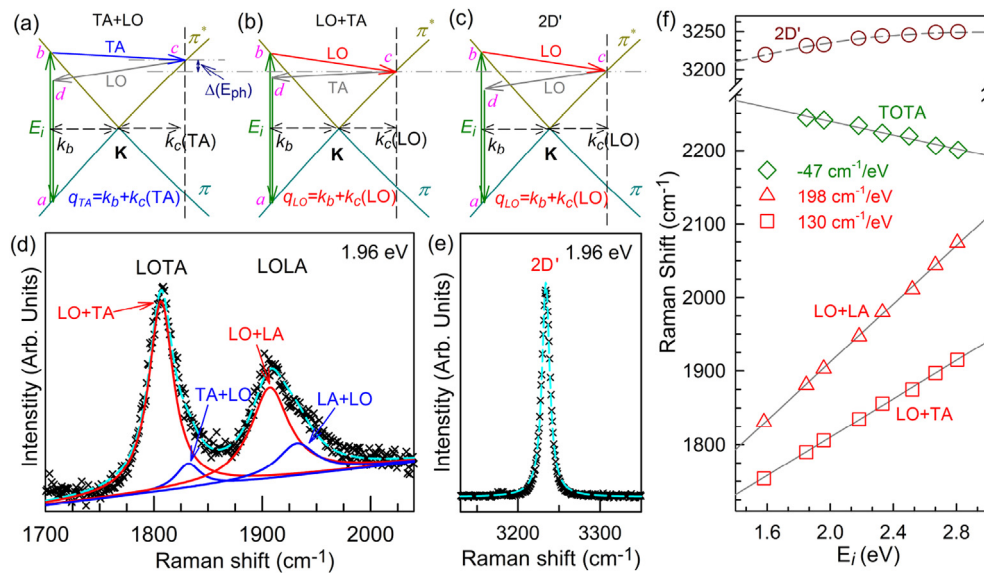
Fig. 2. Evolution of the Raman spectra of graphene with E_i in the spectral ranges of 1650~2300 cm^{-1} and 3150~3300 cm^{-1}. (A colour version of this figure can be viewed online.)

with momentum q_{TA} and energy $\omega_{TA}(q_{TA})$. The electron is further scattered back to a virtual state d by emitting a LO phonon with momentum $-q_{TA}$ and energy $\omega_{LO}(-q_{TA})$, and finally recombines with the hole at the state a. The energy and momentum conservation rules in this process are $E_b - E_c = \omega_{TA}(q_{TA})$ and $k_c(TA) - k_b = q_{TA}$. In combination with the linear electronic bands of graphene with Fermi velocity of v_F, we can obtain $q_{TA} = (E_i - \omega_{TA}(q_{TA}))/v_F$ and the combination mode frequency of $\omega_{TA+LO} = \omega_{TA}(q_{TA}) + \omega_{LO}(-q_{TA})$. $v_F = 5.52 eV\text{Å}$ ($\sim 1.33 \times 10^6 m\,s^{-1}$) is widely taken in the theoretical and experimental works [35,36], which was also taken to calculate the frequency difference of the Stokes and anti-Stokes components of the D and 2D modes in graphene [37]. There is a similar DR Raman process for the LO + TA component as shown in Fig. 3(b). The corresponding combination mode frequency is $\omega_{LO+TA} = \omega_{LO}(q_{LO}) + \omega_{TA}(-q_{LO})$, in which $q_{LO} = (E_i - \omega_{LO}(q_{LO}))/v_F$. The energy difference $\Delta(E_{ph})$ between ω_{TA} and ω_{LO} results in different q_{TA} and q_{LO} in the intravalley DR Raman processes in Fig. 3(a) and (b), respectively, and further results in different frequencies of the TA + LO and LO + TA components, i.e., $\omega_{TA+LO} \neq \omega_{LO+TA}$. Because $\omega_{TA} < \omega_{LO}$, we can obtain $q_{TA} > q_{LO}$, and it is expected that $\omega_{TA+LO} > \omega_{LO+TA}$.

The above analysis on the DR Raman process of the LOTA mode can be applied to the LOLA mode and other combination modes in graphene. Similarly, $\omega_{LA+LO} > \omega_{LO+LA}$. Therefore, both the LOTA and LOLA modes of graphene exhibit a two-peak behavior, which can be fitted by two Lorentzian subpeaks, as demonstrated in Fig. 3(d). The intensities of the LO + TA and LO + LA components are much stronger than those of the TA + LO and LA + LO components, respectively, indicating that electron-phonon coupling for optical phonon branches is much stronger than that of acoustic phonon branches, in line with the previous reports [38,39]. Thus, the LOTA and LOLA bands are dominated by the LO + TA and LO + LA components, whose frequencies can be obtained by fitting the LOTA and LOLA bands, respectively. The DR Raman process of the 2D′ band is depicted in Fig. 3(c). Because the photon-excited electron is firstly scattered by the LO phonon in the LO + TA, LO + LA components and 2D′ mode, the wave vectors of these phonons involved in the DR processes are definitely equal to $|q_{LO}|$ along Γ-M direction for a fixed E_i, so that $\omega_{LO}(q_{LO}) = \omega_{2D'}/2$, which can be directly obtained

and 2300 cm^{-1}, whose frequency exhibits redshift with increasing E_i, showing an opposite dispersion relative to the LOTA and LOLA modes. According to the frequency match and theoretical result [27], it is assigned as the TOTA mode, a combination of TO and TA phonons near the K point, which is associated with intervalley DR Raman process. The expected overtone (2D″ or 2LA) [27] of the LA phonon near the K point is not observed in this work.

The observation of the LOTA, LOLA and 2D′ modes makes it possible to extract the wavevector and frequency of the LA and TA phonons from the LOTA and LOLA modes with asymmetrical lineshapes. We first consider the intravalley DR Raman processes of the LOTA and 2LO (i.e., 2D′) modes in graphene. Fig. 3(a) and (b) demonstrate two possible DR processes of the LOTA mode. For the Raman process of the TA + LO component in Fig. 3(a), an incoming photon with energy E_i can resonantly excite an electron from a state a in the valence band to a state b in the conduction band. The excited electron is scattered to the state c, by emitting a TA phonon

Fig. 3. (a) and (b) Two possible DR Raman processes of the LOTA mode.(c) DR Raman process of the 2D′ mode. The fitting to Raman spectra of the LOTA and LOLA modes (d) and of the 2D′ mode (e) excited by $E_i = 1.96$ eV. (f) Peak positions of the 2D′ (circles) and TOTA (diamonds) modes and the LO + LA (triangles) and LO + TA (squares) components as a function of E_i. Gray curves are the fitting lines to each peak position. (A colour version of this figure can be viewed online.)

by a single Lorentzian peak fitting to the 2D′ mode, as shown in Fig. 3(e). Therefore, the frequencies of TA and LA phonons with $q_{LO} = (E_i - \omega_{2D'}/2)/v_F$ involved in the DR Raman processes of the LO + TA and LO + LA components can be experimentally determined as $\omega_{TA}(q_{LO}) = \omega_{LO+TA} - \omega_{2D'}/2$ and $\omega_{LA}(q_{LO}) = \omega_{LO+LA} - \omega_{2D'}/2$, respectively.

To quantitatively analyze E_i dependence of the LOTA, LOLA and 2D′ modes in Fig. 2(a), these modes are fitted by the Lorentzian lineshape and the results are summarized in Fig. 3(f). The 2D′ mode always can be fitted by a single Lorentzian peak. In contrast to linear E_i-dependent ω_{2D}, quadratic fitting is better for the E_i-dependent $\omega_{2D'}$ as shown by the dashed line in Fig. 3(f), indicating nonlinear phonon dispersion of the LO phonon branch near Γ point. The E_i dependences of the LO + LA and LO + TA components are fitted to be 198 and 130 cm^{-1}/eV, respectively.

Based on the above analysis, $\omega_{TA}(q_{LO})$, $\omega_{LA}(q_{LO})$ and q_{LO} for a specific E_i can be directly determined by the Fermi velocity v_F and experimental data of ω_{LO+TA}, ω_{LO+LA} and $\omega_{2D'}$ excited by E_i. Fig. 4(a) shows the extracted ω_{TA} and ω_{LA} (open triangles and squares) of graphene as a function of E_i and the directly measured ω_{TA} and ω_{LA} (solid triangles and squares) of graphite whisker [20,21]. For a specific E_i, ω_{TA} and ω_{LA} of graphite whisker are slightly higher than those of graphene, indicating the different TA and LA phonon dispersion between them. Fig. 4(b) shows the extracted $\omega_{TA}(q_{LO})$ and $\omega_{LA}(q_{LO})$ from the experimental ω_{LO+TA}, ω_{LO+LA} and $\omega_{2D'}$ as a function of q_{LO}. Because the phonon wave vector with main contribution to Raman intensity is along Γ − M direction ($|k_{\Gamma M}| = 2\pi/\sqrt{3}a$, $a = 2.46$ Å is the lattice constant of graphene) [27], the TA and LA phonon dispersion in Fig. 4(b) is along Γ − M direction. Both the ω_{TA} and ω_{LA} exhibit linear dependence on the wave vector q even though ω_{LA} and ω_{TA} can be as large as ∼450 cm^{-1} and ∼300 cm^{-1}, respectively.

The speed of propagation of an acoustic phonon, which is also the sound velocity (v_{AP}) in the lattice, is given by the slope (α_{AP}, in $cm^{-1}/\frac{2\pi}{a}$) of the acoustic dispersion relation by the relation of $v_{AP} = \alpha_{AP} \times \frac{2\pi}{a} \times 2.998 \times 10^{-3}(km/s)$. Based on the linear phonon dispersion of the TA and LA modes in Fig. 4(b), the in-plane TA and LA sound velocities in graphene can be deduced to be $v_{TA} = 12.9$ km/s and $v_{LA} = 19.9$ km/s. The theoretical calculations with LDA and GGA are also performed to calculate the TA and LA phonon dispersions of graphene, with similar calculation

parameters to previous work [27]. Fig. 4(c) presents the comparison between experimental and theoretical results in the selected range, which reveals the limitation of ab initio calculations using LDA and GGA due to the small phonon energy of the TA and LA phonons in comparison with the LO phonon.

The sound velocities of multilayer graphene (MLG) [6] and graphite [7] have been obtained by different techniques, such as Brillouin scattering, inelastic X-ray scattering and measured Young's modulus. And meanwhile, various theoretical methods have been applied to calculate the sound velocities of graphene [40], graphite [41] and (10,10) armchair carbon nanotube (A-CNT) [40]. All the experimental and theoretical sound velocities of graphene, MLG, graphite and A-CNT are summarized in Table 1. Since the TA mode of A-CNT has both an ″in-cylindrical-plane″ and an ″out-of-cylindrical-plane″ component [40], v_{TA} of A-CNT is much smaller than v_{TA} and v_{LA} of graphene. On the other hand, the LA mode of A-CNT has only an in-plane component mode [40], so that its v_{LA} is comparable to that of graphene. Since MLG and graphite are stacked by graphene layers in certain ways, their sound velocities are close to each other even though the measured techniques are different. From theoretical calculation, the TA and LA branches of graphene and bilayer graphene (2LG) are almost the same [42], which indicates interlayer coupling have little influence on LA and TA branches. However, the experimental v_{TA} and v_{LA} of graphene are about 10% smaller than those of MLG and graphite. Indeed, this can be confirmed by the lower extracted ω_{TA} and ω_{LA} of graphene than the directly measured ones of graphite whisker for a specific E_i. This indicates that the interlayer coupling in MLG and graphite has influence on their v_{TA} and v_{LA}, in contrast to the previous theoretical result [42].

According to the dynamical theory of crystal lattices [43], elastic stiffness (tension) coefficients can be given by in-plane LA and TA

Table 1
The experimental sound velocities (v_{TA} and v_{LA}) of graphene (present work), MLG [6], graphite [7] obtained from different experimental methods (Raman scattering, Brillouin scattering and inelastic X-ray scattering), and the theoretical (Theo.) ones for graphene [40], graphite [41] and A-CNT [40].

Sound velocities	Graphene	MLG	Graphite	A-CNT
Method	Raman (Theo.)	Brillouin	Inelastic X-ray (Theo.)	Theo.
v_{TA} (km/s)	12.9 (15.0)	13.9	14.7 (12.3)	9.43
v_{LA} (km/s)	19.9 (21.0)	21.5	22.2 (21.0)	20.35
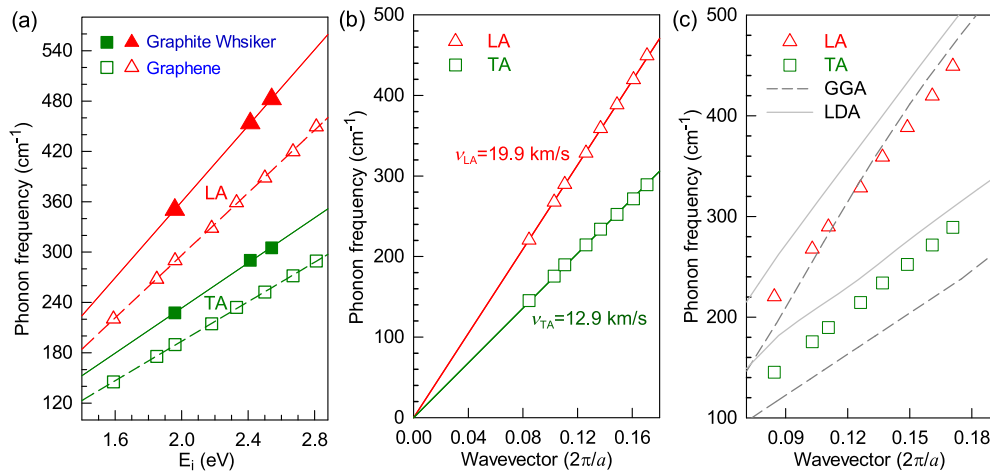
Fig. 4. (a) Extracted frequencies (open triangles and squares) of the TA and LA phonons of graphene from the TALO and LALO combination modes and the directly measured frequencies (solid triangles and squares) of the TA and LA phonons of graphite whisker. (b) Experimentally obtained frequencies of TA and LA phonons of graphene as a function of wave vector. $a = 2.46$ Å is the lattice constant of graphene. The fitted lines start from the original point. (c) The experimental and theoretical results of TA and LA phonon branches in the selected region of wave vector. The theoretical calculations are performed with LDA (solid lines) and GGA (dashed lines). (A colour version of this figure can be viewed online.)

mode velocities. The two-dimensional (2d) elastic stiffness (tension) coefficients have the values of $c_{11} = \rho_{2d} \cdot v_{LA}^2$ and $c_{66} = \rho_{2d} \cdot v_{TA}^2$, where $\rho_{2d} = 7.61 \times 10^{-8}$ g/cm^2 is the surface mass density. Therefore, we can get $c_{11} = 30.13 \times 10^4$ dyn/cm and $c_{66} = 12.66 \times 10^4$ dyn/cm. These values are close to the theoretical result [4] $c_{11} = 40.5 \times 10^4$ dyn/cm and $c_{66} = 15.7 \times 10^4$ dyn/cm. Because graphene is 2d isotropic solid, the expressions of 2d Young's modulus and Poisson's ratio are [44].

$$Y_{2d} = \frac{4B_{2d}\mu_{2d}}{B_{2d} + \mu_{2d}}$$

$$\sigma_{2d} = \frac{B_{2d} - \mu_{2d}}{B_{2d} + \mu_{2d}}$$

where bulk modulus $B_{2d} = c_{11} - c_{66} = 17.47 \times 10^4$ dyn/cm and shear modulus $\mu_{2d} = c_{66} = 12.66 \times 10^4$ dyn/cm [44]. Therefore, we get 2d Young's modulus $Y_{2d} = 29.36 \times 10^4$ dyn/cm, Poisson's ratio $\sigma_{2d} = 0.159$. Considering the thickness (h_g) of graphene as the Van der Waals diameter of carbon atom (0.335 nm), Young's modulus of graphene is obtained as $Y_{2d}/h_g = 0.88$ TPa, which is close to the theoretical result (1.03 TPa) [45] and experimental one (1.0 ± 0.1 TPa) measured by atomic force microscope [46].

4. Conclusion

In summary, the two dominant Raman peaks of graphene in the range between 1700 and 2100 cm^{-1} have been investigated by multiple wavelength excitations, which are assigned as the combination modes of LO phonons with TA and LA phonons by double resonance Raman scattering, respectively. By virtue of the experimental frequency of the 2D′ mode, the phonon dispersions of TA and LA phonon branches have been determined. The TA and LA phonon velocities ($v_{TA} = 12.9$ km/s and $v_{LA} = 19.9$ km/s) can be obtained from a linear fit to the corresponding experimental data. The experimental v_{TA} and v_{LA} of graphene are about ~10% smaller than those of MLG and graphite, indicating that the interlayer coupling in MLG and graphite does have an influence on their sound velocities. Further theoretical calculations and experimental works are necessary to confirm this results. The Young's modulus of graphene is obtained as 0.88 TPa, which is close to the experimental result by atomic force microscope measurement and the theoretical prediction. The Poisson's ratio (0.156) of graphene has been also deduced from its sound velocities.

References

[1] A.C. Ferrari, F. Bonaccorso, V. Falko, K.S. Novoselov, S. Roche, P. Bøggild, et al., Science and technology roadmap for graphene, related two-dimensional crystals, and hybrid systems, Nanoscale 7 (2015) 4598, https://doi.org/10.1039/c4nr01600a.

[2] D. Nika, S. Ghosh, E. Pokatilov, A. Balandin, Lattice thermal conductivity of graphene flakes: comparison with bulk graphite, Appl. Phys. Lett. 94 (20) (2009) 203103, https://doi.org/10.1063/1.3136860.

[3] J.U. Lee, D. Yoon, H. Kim, S.W. Lee, H. Cheong, Thermal conductivity of suspended pristine graphene measured by Raman spectroscopy, Phys. Rev. B 83 (8) (2011), 081419. https://doi.org/10.1103/PhysRevB.83.081419.

[4] K. Michel, B. Verberck, Theory of the evolution of phonon spectra and elastic constants from graphene to graphite, Phys. Rev. B 78 (2008), 085424, https://doi.org/10.1103/PhysRevB.78.085424.

[5] J.U. Lee, D. Yoon, H. Cheong, Estimation of young s modulus of graphene by Raman spectroscopy, Nano Lett. 12 (9) (2012) 4444–4448. https://doi.org/10.1021/nl301073q.

[6] Z. Wang, H. Lim, S. Ng, B. Özyilmaz, M. Kuok, Brillouin scattering study of low-frequency bulk acoustic phonons in multilayer graphene, Carbon 46 (15) (2008) 2133, https://doi.org/10.1016/j.carbon.2008.09.028.

[7] A. Bosak, M. Krisch, M. Mohr, J. Maultzsch, C. Thomsen, Elasticity of single-crystalline graphite: inelastic x-ray scattering study, Phys. Rev. B 75 (15) (2007) 153408, https://doi.org/10.1103/PhysRevB.75.153408.

[8] R. Nicklow, N. Wakabayashi, H. Smith, Lattice dynamics of pyrolytic graphite, Phys. Rev. B 5 (12) (1972) 4951, https://doi.org/10.1103/PhysRevB.5.4951.

[9] J. Wilkes, R. Palmer, R. Willis, Phonons in graphite studied by EELS, J. Electron. Spectrosc. Relat. Phenom. 44 (1) (1987) 355–360, https://doi.org/10.1016/0368-2048(87)87036-6.

[10] C. Oshima, T. Aizawa, R. Souda, Y. Ishizawa, Y. Sumiyoshi, Surface phonon dispersion curves of graphite (0001) over the entire energy region, Solid State Commun. 65 (12) (1988) 1601–1604, https://doi.org/10.1016/0038-1098(88)90660-6.

[11] S. Siebentritt, R. Pues, K.H. Rieder, A.M. Shikin, Surface phonon dispersion in graphite and in a lanthanum graphite intercalation compound, Phys. Rev. B 55 (12) (1997) 7927, https://doi.org/10.1103/PhysRevB.55.7927.

[12] O. Dubay, G. Kresse, Accurate density functional calculations for the phonon dispersion relations of graphite layer and carbon nanotubes, Phys. Rev. B 67 (3) (2003), 035401, https://doi.org/10.1103/PhysRevB.67.035401.

[13] R. Saito, T. Takeya, T. Kimura, G. Dresselhaus, M.S. Dresselhaus, Raman intensity of single-wall carbon nanotubes, Phys. Rev. B 57 (1998) 4145, https://doi.org/10.1103/PhysRevB.57.4145.

[14] L. Malard, M. Pimenta, G. Dresselhaus, M. Dresselhaus, Raman spectroscopy in graphene, Phys. Rep. 473 (5) (2009) 51, https://doi.org/10.1016/j.physrep.2009.02.003.

[15] A.C. Ferrari, D.M. Basko, Raman spectroscopy as a versatile tool for studying the properties of graphene, Nat. Nanotechnol. 8 (4) (2013) 235, https://doi.org/10.1038/nnano.2013.46.

[16] J.B. Wu, M.L. Lin, X. Cong, H.N. Liu, P.H. Tan, Raman spectroscopy of graphene-based materials and its applications in related devices, Chem. Soc. Rev. 47 (2018) 1822–1873, https://doi.org/10.1039/C6CS00915H.

[17] C. Thomsen, S. Reich, Double resonant Raman scattering in graphite, Phys. Rev. Lett. 85 (2000) 5214, https://doi.org/10.1103/PhysRevLett.85.5214.

[18] R. Saito, A. Jorio, A. Souza Filho, G. Dresselhaus, M. Dresselhaus, M. Pimenta, Probing phonon dispersion relations of graphite by double resonance Raman scattering, Phys. Rev. Lett. 88 (2) (2002), 027401, https://doi.org/10.1103/PhysRevLett.88.027401.

[19] D. Mafra, G. Samsonidze, L. Malard, D. Elias, J. Brant, F. Plentz, et al., Determination of LA and TO phonon dispersion relations of graphene near the Dirac point by double resonance Raman scattering, Phys. Rev. B 76 (23) (2007) 233407, https://doi.org/10.1103/PhysRevB.76.233407.

[20] P. Tan, C. Hu, J. Dong, W. Shen, B. Zhang, Polarization properties, high-order Raman spectra, and frequency asymmetry between Stokes and anti-Stokes scattering of Raman modes in a graphite whisker, Phys. Rev. B 64 (2001) 214301, https://doi.org/10.1103/PhysRevB.64.214301.

[21] P. Tan, L. An, L. Liu, Z. Guo, R. Czerw, D.L. Carroll, et al., Probing the phonon dispersion relations of graphite from the double-resonance process of Stokes and anti-Stokes Raman scatterings in multiwalled carbon nanotubes, Phys. Rev. B 66 (2002) 245410, https://doi.org/10.1103/PhysRevB.66.245410.

[22] S. Bernard, E. Whiteway, V. Yu, D. Austing, M. Hilke, Probing the experimental phonon dispersion of graphene using ^{12}C and ^{13}C isotopes, Phys. Rev. B 86 (8) (2012), 085409, https://doi.org/10.1103/PhysRevB.86.085409.

[23] C. Cong, T. Yu, R. Saito, G.F. Dresselhaus, M.S. Dresselhaus, Second-order overtone and combination Raman modes of graphene layers in the range of 1690–2150 cm^{-1}, ACS Nano 5 (3) (2011) 1600–1605, https://doi.org/10.1021/nn200010m.

[24] R. Rao, R. Podila, R. Tsuchikawa, J. Katoch, D. Tishler, A. Rao, et al., Effects of layer stacking on the combination Raman modes in graphene, ACS Nano 5 (3) (2011) 1594–1599, https://doi.org/10.1021/nn1031017.

[25] K. Sato, J. Park, R. Saito, C. Cong, T. Yu, C. Lui, et al., Raman spectra of out-of-plane phonons in bilayer graphene, Phys. Rev. B 84 (03) (2011), 035419, https://doi.org/10.1103/PhysRevB.84.035419.

[26] Q.Q. Li, X. Zhang, J.B. Wu, Y. Lu, P.H. Tan, Z.H. Feng, et al., The second-order combination Raman modes of bilayer graphene in the range of 1800-2150 cm^{-1}, Acta Phys. Sin. 63 (14) (2014) 147802, https://doi.org/10.7498/aps.63.147802.

[27] P. Venezuela, M. Lazzeri, F. Mauri, Theory of double-resonant Raman spectra in graphene: intensity and line shape of defect-induced and two-phonon bands, Phys. Rev. B 84 (2011), 035433, https://doi.org/10.1103/PhysRevB.84.035433.

[28] W. Zhao, P. Tan, J. Zhang, J. Liu, Charge transfer and optical phonon mixing in few-layer graphene chemically doped with sulfuric acid, Phys. Rev. B 82 (24) (2010) 245423, https://doi.org/10.1103/PhysRevB.82.245423.

[29] P. Giannozzi, S. Baroni, N. Bonini, M. Calandra, R. Car, C. Cavazzoni, et al., QUANTUM ESPRESSO: a modular and open-source software project for quantum simulations of materials, J. Phys. Condens. Matter 21 (39) (2009) 395502, https://doi.org/10.1088/0953-8984/21/39/395502.

[30] P. Giannozzi, O. Andreussi, T. Brumme, O. Bunau, M.B. Nardelli, M. Calandra, et

al., Advanced capabilities for materials modelling with QUANTUM ESPRESSO, J. Phys. Condens. Matter 29 (46) (2017) 465901, https://doi.org/10.1088/1361-648X/aa8f79.

[31] P.E. Blöchl, Projector augmented-wave method, Phys. Rev. B 50 (24) (1994) 17953, https://doi.org/10.1103/PhysRevB.50.17953.

[32] G. Kresse, D. Joubert, From ultrasoft pseudopotentials to the projector augmented-wave method, Phys. Rev. B 59 (3) (1999) 1758, https://doi.org/10.1103/PhysRevB.59.1758.

[33] S. Reich, C. Thomsen, Raman spectroscopy of graphite, Phil. Trans. Roy. Soc. Lond. 362 (2004) 2271–2288, https://doi.org/10.1098/rsta.2004.1454.

[34] M. Lazzeri, C. Attaccalite, L. Wirtz, F. Mauri, Impact of the electron-electron correlation on phonon dispersion: failure of LDA and GGA DFT functionals in graphene and graphite, Phys. Rev. B 78 (2008), 081406, https://doi.org/10.1103/PhysRevB.78.081406.

[35] S. Pisana, M. Lazzeri, C. Casiraghi, K.S. Novoselov, A.K. Geim, A.C. Ferrari, et al., Breakdown of the adiabatic Born–Oppenheimer approximation in graphene, Nat. Mater. 6 (3) (2007) 198, https://doi.org/10.1038/nmat1846.

[36] C. Faugeras, S. Berciaud, P. Leszczynski, Y. Henni, K. Nogajewski, M. Orlita, et al., Landau level spectroscopy of electron-electron interactions in graphene, Phys. Rev. Lett. 114 (12) (2015) 126804, https://doi.org/10.1103/PhysRevLett.114.126804.

[37] X. Cong, J.B. Wu, M.L. Lin, X.L. Liu, W. Shi, P. Venezuela, et al., Stokes and anti-Stokes Raman scattering in mono- and bilayer graphene, Nanoscale 10 (2018) 16138–16144, https://doi.org/10.1039/C8NR04554B.

[38] S. Piscanec, M. Lazzeri, F. Mauri, A. Ferrari, J. Robertson, Kohn anomalies and electron-phonon interactions in graphite, Phys. Rev. Lett. 93 (18) (2004) 185503, https://doi.org/10.1103/PhysRevLett.93.185503.

[39] D. Basko, S. Piscanec, A. Ferrari, Electron-electron interactions and doping dependence of the two-phonon Raman intensity in graphene, Phys. Rev. B 80 (16) (2009) 165413, https://doi.org/10.1103/PhysRevB.80.165413.

[40] R. Saito, T. Takeya, T. Kimura, G. Dresselhaus, M. Dresselhaus, Raman intensity of single-wall carbon nanotubes, Phys. Rev. B 57 (7) (1998) 4145, https://doi.org/10.1103/PhysRevB.57.4145.

[41] M. Dresselhaus, G. Dresselhaus, K. Sugihara, I. Spain, H. Goldberg, Graphite Fibers and Filaments, vol. 5, Springer-Verlag, Berlin, 1988, https://doi.org/10.1007/978-3-642-83379-3.

[42] S. Ghosh, W. Bao, D.L. Nika, S. Subrina, E.P. Pokatilov, C.N. Lau, et al., Dimensional crossover of thermal transport in few-layer graphene, Nat. Mater. 9 (7) (2010) 555, https://doi.org/10.1038/nmat2753.

[43] M. Born, K. Huang, Dynamical Theory of Crystal Lattices, Oxford University Press, New York, 1954.

[44] P. Chaikin, T. Lubensky, Principles of Condensed Matter Physics, vol. 1, Cambridge university press, 1995.

[45] G. Lier, C. Alsenoy, V. Doren, P. Geerlings, Ab initio study of the elastic properties of single-walled carbon nanotubes and graphene, Chem. Phys. Lett. 326 (1) (2000) 181, https://doi.org/10.1016/S0009-2614(00)00764-8.

[46] C. Lee, X. Wei, J. Kysar, J. Hone, Measurement of the elastic properties and intrinsic strength of monolayer graphene, Science 321 (5887) (2008) 385, https://doi.org/10.1126/science.1157996.